

Resonant bio- and chemical sensors using low-refractive-index-contrast liquid-core Bragg fibers

Hang Qu, Maksim Skorobogatiy*

Department of Engineering Physics, Ecole Polytechnique de Montréal, C.P. 6079, succ. Centre-ville, Montréal, Québec, Canada H3C 3A7¹

ARTICLE INFO

Article history:

Received 10 May 2009

Received in revised form

24 September 2011

Accepted 12 October 2011

Available online 20 November 2011

Keywords:

Resonant sensors

Bragg fibers

Photonic bandgap fibers

ABSTRACT

We review design principles and experimental realization of the resonant sensors that use low-refractive-index-contrast Bragg fibers filled with liquid analytes. Such fibers have been recently demonstrated using polymer/polymer, glass/air and polymer/air material combinations. Low-refractive-index-contrast Bragg fibers have narrow bandgaps whose spectral position is highly sensitive to the value of the real part of the analyte refractive index filling the fiber core. We demonstrate theoretically and experimentally that when Bragg fiber is operated in the radiation loss dominated regime it can be used as a highly sensitive sensor of changes in the real part of the analyte refractive index. The experimental sensitivity of the proposed sensor is ~ 1400 nm/RIU, which is comparable to those of the waveguide-based plasmonic sensors. Finally, we experimentally explore the possibility of using low-refractive-index-contrast Bragg fibers to detect changes in thicknesses of thin layers deposited directly on the inner surface of the fiber core. A moderate sensitivity of ~ 0.9 nm/ μm is reported due to the poor overlap between core guided modes and the coated layer.

© 2011 Elsevier B.V. All rights reserved.

1. Introduction

R&D into fiber-optic bio- and chemo-sensors (FOS) has made a lot of progress during the last 10 years. This is due to the appealing properties of FOS such as immunity to electromagnetic interference, safety in explosive environments, and potential to provide continuous quantitative and qualitative real-time analysis. Chemically sensitive thin films deposited on selected areas of optical fibers can influence the propagation of light in such fibers depending on the presence or the absence of chemical molecules in the surrounding environment [1]. A wide range of optical sensors has been developed for selective bio-molecule detection [2,3]. Most of them have reliability issues as they employ very fragile antibodies as sensing elements. These sensors include high refractive index waveguides [4], surface plasmon resonance sensors [5], resonant mirrors [6], and classical fiber-optical sensors [7,8]. Most optical sensors are based on evanescent wave sensing, where the perturbations in the refractive index close to the sensor surface are probed by the exponentially decaying optical wave. Such sensors have proven to be highly sensitive in detection of small targets such as proteins and viruses, but they experience difficulties in detecting larger targets such as bacteria (0.5–5 μm) since in that case much

larger penetration of the evanescent field into analyte is required [9].

To date, most of fiber-optic biosensors have utilized label-based sensing strategies in which the target analytes are attached (labeled) with fluorescent or radioactive tags before detection. Thus, detection of the radiation (fluorescence) intensity of the attached labels could provide quantitative information of the target analytes. Though label-based detections have shown high sensitivities in some biosensing applications, the process of labeling target analytes is time-consuming and the cost of labels is high. Furthermore, the labeling strategies potentially have synthetic challenges, multiple label issues, and may block the important active site on the bound analytes, thus leading to modification of the analyte functionalities. Due to these considerations, “label-free” sensing strategies have recently attracted plenty of scientific attention. Typical label-free fiber-optic sensors detect shifts of the resonant wavelength in response to resonant structure changes caused by the presence of bio-analyte layers [10,11]. Without the need of labeling test analytes, label-free sensors enable on-site and real-time detections, which is an advantage to emerging point-of-care applications. However, challenges of the label-free detections include development of proper bio-recognition elements (such as enzymes, antibodies, and phages) that can bind specifically to target bio-analytes, and design of the bio-functionalization protocol on the resonant surface of the sensor. Finally, we note that label-free detections typically operate on the “surface” sensing modality in which the measured spectral shift is related to the changes in

* Corresponding author.

E-mail address: maksim.skorobogatiy@polymtl.ca (M. Skorobogatiy).

¹ <http://www.photonics.phys.polymtl.ca/>.

analyte density on the sensor surface rather than the total analyte amount. As to label-based detections, they generally employ the “bulk” sensing modality to detect the total amount of analytes. In summary, when designing the sensing protocol, one has to consider these differences between label-based and label-free sensing strategies to choose the most appropriate method.

Microstructured optical fibers (MOFs), and photonic bandgap (PBG) fibers which are a subset of MOFs, promise a viable technology for the mass production of highly integrated and intelligent sensors in a single manufacturing step [12]. In standard total internal reflection (TIR) fiber-based evanescent-wave sensors the fiber polymer jacket is stripped and the fiber cladding is polished to the core in order to obtain an overlap between the optical field and analyte, with sensor sensitivity proportional to such an overlap. Compared to the conventional solid core optical fibers, MOFs offer a number of unique advantages in sensing applications. A defining feature of a microstructured fiber is the presence of air holes running along its entire length. Fiber optical properties are then determined by the size, shape, and relative position of the holes. Particularly, a unique ability of MOFs is to accommodate biological and chemical samples in gaseous or liquid forms inside of the air holes in the immediate vicinity of the fiber core [13–15]. In this context a MOF is used simultaneously as a light guide and as a fluidic channel. The MOF's unique architecture makes it a very promising sensing platform for chemical and biological detection. First, MOFs naturally integrate optical detection with the microfluidics, allowing for continuous on-line monitoring of dangerous samples in real-time without exposing the personnel to danger. In addition, the samples can be transferred in the enclosed MOF optofluidic system for further confirmation analysis, e.g. polymerase chain reactions (PCR) if needed. Such channels can be further functionalized with bio-recognition layers that can bind and progressively accumulate target biomolecules, thus enhancing sensor sensitivity and specificity. Second, the MOF hole size is in sub-100 μm range, leading to very small fluid samples required for sensing. Third, MOF based sensors can be coiled into long sensing cells ($\sim 10\text{m}$), thus dramatically increasing their sensitivity. The same is impossible to achieve with traditional TIR fiber sensors as side polishing step limits sensor length to several cm. Forth, the desired MOFs can be mass-produced using commercial fiber draw tower in a very cost-effective manner. Fifth, the MOFs can potentially be scaled up into a two-dimensional array with small dimensions, which is suitable for making into portable point-of-care devices for simultaneous on-site detection of different kinds of analytes. Sixth, photonic bandgap fibers can be designed to guide light directly in their analyte-field hollow cores [16]. In such fibers light-analyte coupling is considerably stronger than that in evanescent sensors.

In this paper, we review design principles and experimental realization of the liquid-core fiber sensors using all-polymer low-refractive-index-contrast Bragg fibers. We demonstrate that the Bragg fiber sensor operating on the resonant sensing mode can be used for detection of both “bulk” and “surface” variations of analytes. Firstly, we study sensing of changes in real part of the “bulk” refractive index of the analyte filling the fiber core, and show very high sensitivities $\sim 1400\text{nm}/\text{RIU}$ which are comparable to those of the surface plasmon resonance sensors. High “bulk” sensitivity of our sensors is due to an almost perfect overlap between analytes and optical modes of a sensor, and a resonant nature of the photonic bandgap guidance mechanism. Secondly, we study sensing of changes in the thickness of the thin layers deposited directly on the inner surface of a hollow core. This constitutes a “surface” sensing modality for our sensors. Because of the low overlap between the analyte layer and optical field of a sensor, only modest sensitivities ($\sim 0.9\text{nm}/\mu\text{m}$) to changes in the layer thickness are measured. We, therefore, believe that the

sensors in this work are most relevant when precise refractive index diagnosis for liquids or their mixtures is required.

2. Resonant sensor design principles

In this paper we detail design principles behind a resonant optical sensor utilizing low-refractive-index-contrast analyte-filled Bragg fibers. In resonant sensors one typically employs fibers with strongly non-uniform spectral transmission characteristics that are sensitive to changes in the real part of the analyte refractive index. Moreover, if narrow absorption lines are present in the analyte transmission spectrum, due to Kramers–Kronig relation this will also result in strong variation in the real part of the refractive index in the vicinity of an absorption line. Therefore, resonant sensors allow detection of minute changes both in the real part of the analyte refractive index, as well as in the imaginary part of the analyte refractive index in the vicinity of absorption lines. Although the operational principle of almost all fiber-based resonant sensors relies on strong sensitivity of the fiber transmission losses to the value of the analyte refractive index, particular transduction mechanism for bio-detection can vary. Consider, in particular, the case of a hollow core PBG fiber featuring an analyte filled core. In one sensor implementation one can label the target bio-molecules with highly absorbing particles of known absorption spectra, such as metal nano-particles or quantum dots. The presence of such particles in the aqueous fiber core can then be quantified by detecting appearance of the absorption lines in the fiber transmission spectrum, or through resonant changes in the fiber transmission losses induced by variations in the real part of the core refractive index. In another implementation, a functional layer that binds specific bio-molecules can be deposited on the inside of the hollow fiber core. Bio-molecule binding events to such a layer can then be detected through resonant changes in the fiber transmission losses induced by variations in the real part of the layer refractive index.

Operation of a resonant Bragg fiber-based sensor relies on changes in the radiation loss of a leaky core mode due to changes in the real part of an analyte refractive index. Such a leaky mode is typically confined inside an analyte filled fiber core by a resonant reflector cladding. The term “leaky mode” generally refers to the guidance mechanism where the effective refractive index of a propagating mode is smaller than that of the fiber cladding. Such unusual modes are called leaky modes as, outside of a waveguide core, they do not exhibit a traditional evanescent decay into the cladding, but rather they radiate slowly (leak) into the cladding. Unlike in the case of common TIR fibers, leaky modes in PBG fibers are confined by the bandgap of a microstructured reflector. For a particular value of an analyte refractive index geometry of such a fiber is chosen to provide strong optical confinement of the leaky core mode. An example of a resonant sensor described above is a photonic bandgap fiber featuring a hollow core filled with analyte. When changing the real part of an analyte refractive index, resonant condition for mode confinement will change, resulting in strong changes in the modal radiation loss (see Fig. 1). Detection of changes in the transmitted intensities can be then re-interpreted in terms of the changes in the real part of an analyte refractive index.

3. Detection strategies for absorption-based sensors

We now remind the reader some general facts about amplitude-based and spectral based detection methodologies. Particularly, we focus on fiber-based sensors that rely on detection of changes in the transmitted light intensity in the presence of a target analyte.

In the amplitude-based detection methodology one operates at a fixed wavelength λ and records changes in the amplitude of a signal, which are then re-interpreted in terms of changes in the analyte

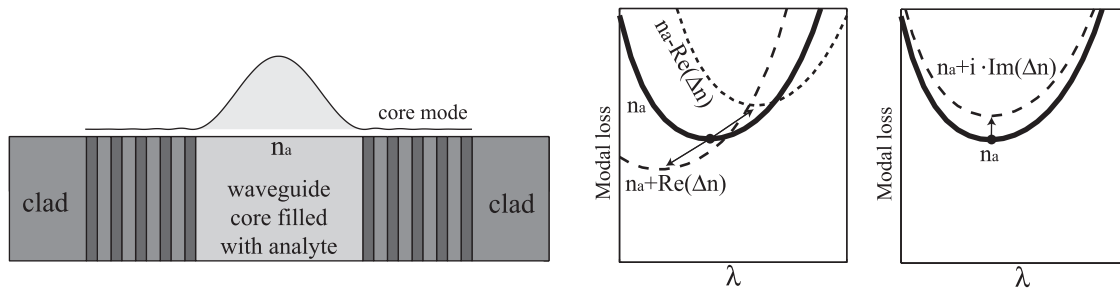


Fig. 1. Operational principle and schematics of the analyte-filled hollow photonic bandgap fiber-based sensor. Transmission loss through such a sensor is very sensitive to the values of both the real and the imaginary parts of the analyte refractive index.

refractive index. To characterize sensitivity of a fiber-based sensor of length L , one employs an amplitude sensitivity function $S_a(\lambda, L)$, which is defined as a relative change in the intensity $P(\delta, \lambda, L)$ of a transmitted light for small changes in the measurand δ . Note that δ can be any parameter that influences transmission properties of a fiber sensor. This includes concentration of absorbing particles in the analyte, thickness of a bio-layer that can change due to capture of specific bio-molecules, as well as real or imaginary parts of the analyte refractive index. Amplitude sensitivity is then defined as:

$$S_a(\lambda, L) = \lim_{\delta \rightarrow 0} \frac{P(\delta, \lambda, L) - P(0, \lambda, L)}{\delta \cdot P(0, \lambda, L)} = \frac{\partial P(\delta, \lambda, L) / \partial \delta}{P(0, \lambda, L)} \Big|_{\delta=0}. \quad (1)$$

Denoting, $\alpha(\delta, \lambda)$ to be the fiber propagation loss at a fixed value δ of a measurand, light intensity at the fiber output can be written as:

$$P(\delta, \lambda, L) = P_{in}(\lambda) \exp(-\alpha(\delta, \lambda)L), \quad (2)$$

where $P_{in}(\lambda)$ is the light intensity launched into a fiber. Substituting (2) into (1), amplitude sensitivity function can be then expressed as:

$$S_a(\lambda, L) = - \frac{\partial \alpha(\delta, \lambda)}{\partial \delta} \Big|_{\delta=0} \cdot L. \quad (3)$$

As follows from (3), sensor sensitivity is proportional to the sensor length L . In turn, as follows from (2), the maximal sensor length is limited by the absorption loss of a fiber. Defining $P_{det}(\lambda)$ to be the power detection limit at which changes in the light intensity can still be detected reliably, the maximal sensor length allowed by the power detection limit can be calculated from (2) as:

$$L = \frac{\log(P_{in}(\lambda)/P_{det}(\lambda))}{\alpha(0, \lambda)}. \quad (4)$$

Defining $\eta_{det}(\lambda) = \log(P_{in}(\lambda)/P_{det}(\lambda))$, maximal sensitivity allowed by the power detection limit can be written using (3) as:

$$S_a(\lambda) = -\eta_{det}(\lambda) \frac{\partial \alpha(\delta, \lambda) / \partial \delta}{\alpha(0, \lambda)} \Big|_{\delta=0}. \quad (5)$$

In all the simulations that follow we assume that $\eta_{det}(\lambda) = 1$, which allows us to characterize an inherent sensitivity of a sensor system, while separating it from the issue of a power budget that might bring additional sensitivity enhancement. Finally, given sensor amplitude sensitivity, to estimate sensor resolution of a measurand δ , one can use expression (1). Assuming that the minimal detectable relative change in the signal amplitude is $(\Delta P/P)_{min}$ (which is typically on the order of 1% if no advanced electronics is used), then the minimum value of a measurand that can be detected by such a sensor is:

$$\delta_{min} = \frac{(\Delta P/P)_{min}}{S_a(\lambda)}. \quad (6)$$

Another popular sensing methodology is spectral-based. It uses detection of displacements of spectral singularities in the presence

of a measurand with respect to their positions for a zero level of a measurand. This sensing approach is particularly effective in the resonant sensor configurations that feature sharp transmission or absorption peaks in their spectra. Defining $\lambda_p(\delta)$ to be the position of a peak in a sensor transmission spectrum as a function of a measurand value δ , spectral sensitivity function can be defined as:

$$S_\lambda = \frac{\partial \lambda(\delta)}{\partial \delta} \Big|_{\delta=0}. \quad (7)$$

Given sensor spectral sensitivity, to estimate sensor resolution of a measurand δ , one can use expression (7). Thus, assuming that the minimal detectable spectral shift in the peak position is $(\Delta \lambda_p)_{min}$ (which is typically on the order of 0.1 nm in the visible spectral range if no advanced optical detection is used), then the minimum value of a measurand that can be detected by such a sensor is:

$$\delta_{min} = \frac{(\Delta \lambda_p)_{min}}{S_\lambda}. \quad (8)$$

4. Sensing using analyte-filled hollow core photonic bandgap fibers

We now describe the resonant sensor based on hollow core photonic bandgap fibers filled with analyte. In their cross-section PBG fibers can contain periodic sequence of micron-sized layers of different materials [17,18] (Fig. 2(a)), periodically arranged micron-sized air voids [19–21] (Fig. 2(b)), or rings of holes separated by nano-supports [22,23] (Fig. 2(c)). PBG fibers are currently available in silica glass, polymer and specialty soft glass implementations. The key functionality of such fibers is their ability to guide light directly in the hollow or liquid-filled cores with refractive index smaller than the refractive index of a surrounding cladding material. Unlike microstructured fibers, PBG fibers confine light in their hollow cores by photonic bandgap effect, rather than by total internal reflection. Practically, bandgaps are defined as frequency regions of enhanced fiber transmission, and they are the result of destructive interference of the core guided light inside of the fiber microstructured cladding. When launching spectrally broad light into a PBG fiber, only the spectral components guided by the fiber bandgaps will reach the fiber end, while all the spectral components not located within the bandgaps will be irradiated out near the fiber coupling end. Moreover, even in the absence of fiber material losses, core guided modes always exhibit radiation loss. This is a direct consequence of guidance in a core with refractive index smaller than that of a cladding. As we will soon see, core mode radiation loss can be very sensitive to the value of the real part of the refractive index of the material filling the fiber core, which can be utilized for sensor applications. Finally, PBG fibers have a tendency to improve the beam quality of guided light, while being effectively single mode in the limit of long propagation distances. This is a consequence of the fact that radiation losses (and, generally, absorption losses too) of the core guided modes of a PBG fiber

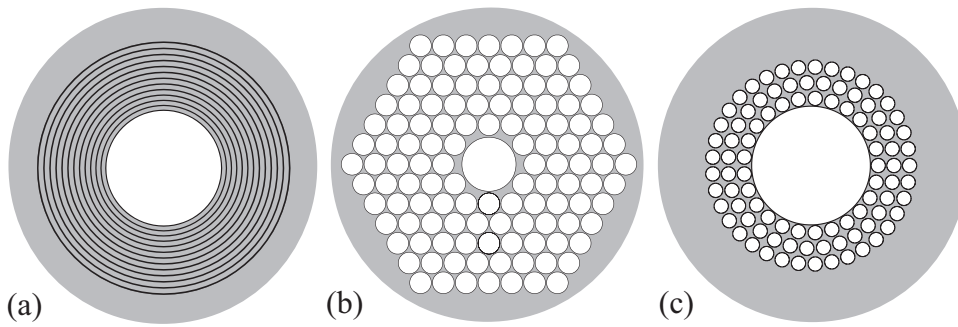


Fig. 2. Various types of hollow core photonic bandgap fibers. (a) Bragg fiber featuring large hollow core surrounded by a periodic sequence of high and low refractive index layers. (b) Photonic crystal fiber featuring small hollow core surrounded by a periodic array of large air holes. (c) Microstructured fiber featuring medium size hollow core surrounded by several rings of small air holes separated by nano-size bridges.

are strongly differentiated with only a few low-order modes having small propagation losses. Thus, when exciting several modes at the fiber input end, only the modes having the lowest losses will survive till the fiber end. For historical reference we mention that before the invention of the all-dielectric PBG fibers, guidance in the hollow core fibers has been demonstrated in the context of metal coated capillaries [24,25].

We now detail some of the advantages offered by the hollow core PBG fibers for sensing applications. One has to distinguish two modes of operation of such sensors. The first is the non-resonant sensing mode in which sensing of changes in imaginary part of the analyte refractive index (analyte absorption) is performed by detecting the presence and strength of the narrow absorption bands in the fiber transmission spectrum. This is the simplest, non-resonant application of the hollow PBG fibers for optical sensing in which one only takes advantage of large overlap of the core guided leaky mode with analyte. In such sensors, signal strength due to analyte absorption, as well as sensor sensitivity are directly proportional to the sensor length. Recently, several experimental implementations of such absorption-based sensors have been demonstrated [26–30]. The second is the resonant sensing mode in which sensing of changes in the real part of analyte refractive index filling the PBG fiber core and sensing of changes in thicknesses of layers deposited on the inner surface of fiber core are performed by detecting the shift of resonant wavelength in the fiber transmission. As we explained in the following section, the sensitivity of the PBG fiber sensor operating in the resonant mode is virtually independent to the fiber length.

4.1. Non-resonant sensing

Classic perturbation theory considerations [31] predicts that changes in the effective refractive index of a guided mode Δn_{eff} are related to the changes in the refractive index Δn_a of analyte infiltrating the fiber, through the overlap factor f defined as:

$$\Delta n_{eff} = \Delta n_a \cdot f = \text{Re}(\Delta n_a) \cdot f + i \cdot \text{Im}(\Delta n_a) \cdot f \quad f = \frac{\int_{\text{analyte}} dA |\mathbf{E}|^2}{\text{Re} \left(\hat{\mathbf{z}} \cdot \int_{\text{crosssection}} dA \mathbf{E}_t^* \times \mathbf{H}_t \right)}, \quad (9)$$

where \mathbf{E}_t , \mathbf{H}_t are the transverse electro-magnetic fields of a fiber mode, while \mathbf{E} is a complete electric field of a mode. Strictly speaking, expression (9) is only valid for the truly guided square integrable modes of the total internal reflection (TIR) fibers. In the case of hollow-core PBG fibers the leaky modes are, generally, non-square integrable [32]. In this case, however, expression (9) can still be used but only approximately. Particularly, to avoid divergence in the denominator of (9), one performs integration only over the finite fiber crosssection limited by the interface between

the multilayer reflector and a cladding. For the hollow core PBG fibers, detailed simulations show that f is typically larger than 0.9. The value of an overlap increases rapidly when the fiber core size increases, reaching values higher than 0.99 for even the moderate core sizes $R_{\text{core}} \sim 5\text{--}10\lambda$. Such a high value of the overlap factor is explained by high confinement of the guided mode in the fiber core (see, for example, energy flux distribution of the core guided mode in the inset of Fig. 1).

Expression (9) is fundamental for the analysis of non-resonant absorption-based sensors. Consider, for example, a microstructured or a hollow core fiber filled with aqueous solution. One possible biosensor implementation utilizing such fibers can, for example, monitor presence and concentration of specific biomolecules labeled by highly absorbing nano-particles. In such a sensor biomolecules in the aqueous solution are purged through the fiber microstructure. Defining C to be the concentration (measurand; $\delta = C$ in (1)) of the absorbing particles mixed with analyte, and assuming that nano-particle bulk absorption per unit of concentration is $\alpha_c(\lambda)$, while fiber loss in the absence of nano-particles is $\alpha_f(\lambda)$, then total fiber loss in the presence of absorbing nano-particles can be written using (9) as:

$$\alpha(C, \lambda) = \alpha_f(\lambda) + f \cdot C \cdot \alpha_c(\lambda). \quad (10)$$

In derivation of (10) we used the fact that $\text{Im}(\Delta n_a) \sim C \cdot \alpha_c$, $\alpha(C, \lambda) \sim \text{Im}(n_{eff})$. By substituting (10) into (5), we now find expression for the maximal non-resonant sensor sensitivity to changes in the nano-particle concentration:

$$S_a(\lambda) = -f \frac{\alpha_c(\lambda)}{\alpha_f(\lambda)}. \quad (11)$$

Note that as nano-particle absorption $\alpha_c(\lambda)$ is completely independent from the fiber loss $\alpha_f(\lambda)$ in the absence of nano-particles, sensitivity (11) of a non-resonant sensor is, thus, directly proportional to the fiber length $L \sim 1/\alpha_f(\lambda)$. Consequently, to increase sensor sensitivity one has to simply work with longer fibers featuring low propagation loss.

4.2. Resonant sensing

4.2.1. Sensing of changes in real part of analyte refractive index

Note that expression (9), when applied to PBG fibers, does not account for the spectral shift of the PBG fiber bandgap (see Fig. 1) due to changes in the real part of the refractive index of an analyte filling the fiber core. In fact, for the hollow-core PBG fibers in place of (9) one has to use the following modified expression:

$$\Delta n_{eff} = \text{Re}(\Delta n_a) \cdot f + i[\text{Im}(\Delta n_a) \cdot f + \text{Re}(\Delta n_a) \cdot f_{rad}] \quad (12)$$

Here, f_{rad} is a radiation factor that describes changes in the radiation losses of a photonic bandgap guided mode due to spectral shift of

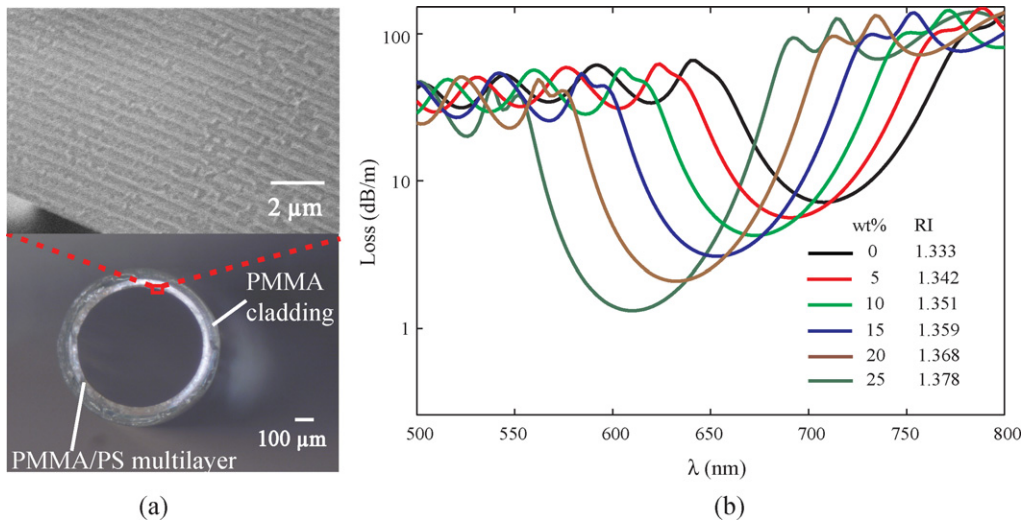


Fig. 3. (a) Bottom: cross section of the hollow core Bragg fiber; top: SEM figure of the PMMA/PS multilayer in the Bragg reflector; (b) simulated loss spectra of the Bragg fiber filled with NaCl solutions of different concentrations. The weight concentrations (wt.%) and corresponding refractive indices of the NaCl solutions are given in the inset of (b).

a fiber bandgap caused by changes in the real part of the refractive index of an analyte filling the fiber core.

To understand the radiation loss contribution in (12) one has to recall the principles of design and operation of the hollow-core PBG fibers. Consider, as an example, the case of an all-polymer low-refractive-index-contrast Bragg fiber featuring a water filled core (refractive index n_c) surrounded by a Bragg reflector (Fig. 3(a)) made of a periodic multilayer of polymethyl methacrylate (PMMA)/polystyrene (PS) [18] with the real parts of refractive indices to be n_l and n_h (n_l/n_h : 1.487/1.581 @ 650 nm). From the basic theory of low-refractive-index-contrast Bragg fibers, the center wavelength, λ_c , of the fundamental reflector bandgap could be approximately calculated by [33]:

$$\frac{\lambda_c}{2} = [d_h(n_h^2 - n_c^2)^{1/2} + d_l(n_l^2 - n_c^2)^{1/2}], \quad (13)$$

where d_l , d_h are the thicknesses of the low- and high-index layer in the Bragg reflector. From (13), variations in the real part of refractive index filling the core could modify the resonant condition of the Bragg fiber, thus leading to changes in the center positions of the fiber bandgap, which constitutes the sensing mechanism of a Bragg fiber sensor.

To verify the resonant sensing mechanism, we now perform a simulation based on transfer matrix method (TMM) [32] to calculate the loss spectra of the fundamental Gaussian-like HE_{11} mode of the Bragg fiber. In fact, HE_{11} mode plays a key role in the operation of a majority of the hollow-core based sensors as it is the easiest mode to excite with an external Gaussian-like laser source. To perform the simulation, we measure the refractive indices of PMMA and PS using a VASE Ellipsometer (J.A. Woollam. Co. Inc.). The average thicknesses (d_l , d_h) of each layer in the Bragg reflector are 0.37 μm and 0.13 μm measured from the SEM (scanning electron microscope) figures (Fig. 3(a)). The number of bi-layers in the Bragg reflector is approximately to be 25. As liquid analytes, we choose a series of NaCl solutions with the weight concentrations ranging from 0% to 25% with a 5% increment step. Real parts of refractive indices of the NaCl solutions can be found elsewhere [34], and the bulk absorption of NaCl solutions is assumed to be identical to that of pure water [35]. Therefore, in our simulation we compute the total loss of an HE_{11} mode taking into account absorption loss of water, as well as dispersion of water and plastics in the Bragg reflector. Note that in our simulation we assume that the absorption coefficients of NaCl solutions change negligibly by increasing

the concentration of NaCl [35], thus the variations in propagation loss of the Bragg fiber are only attributed to the changes in real part of analyte refractive index. Results of the TMM simulation (Fig. 3(b)) suggest that the bandgap of the fiber reflector features a blue-shift as the real part of analyte refractive index increases. For comparison, we plot in Fig. 4 the spectral shift of the bandgap center wavelength calculated from Eq. (13) and obtained from the TMM simulation. An excellent agreement is found between the two data sets.

We now investigate the spectral sensitivity of the Bragg fiber sensor to changes in real part of the analyte refractive index filling the fiber core. By substituting (13) into (7), we find the theoretical expression of the spectral sensitivity of the Bragg fiber sensor as:

$$S = \left| \frac{\partial \lambda_c}{\partial n_c} \right| = 2 \left[d_h \left(\frac{n_h^2}{n_c^2} - 1 \right)^{-1/2} + d_l \left(\frac{n_l^2}{n_c^2} - 1 \right)^{-1/2} \right]. \quad (14)$$

From (14), we note that the sensitivity of a Bragg fiber sensor increases with the increasing refractive index of an analyte filling the fiber core. Consequently, the shift of resonant wavelength should have a polynomial dependence on the increasing analyte refractive index. However, within the relatively small dynamic range (n_c : 1.333–1.378) of our simulation, we can approximately consider the shift of resonant wavelength (bandgap center) to be linearly dependent on the increment of the refractive index of the core. From the linear fitting in Fig. 4 the simulated sensitiv-

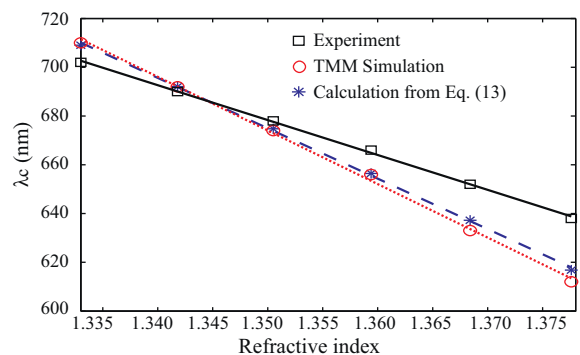


Fig. 4. Comparison of the spectral shifts obtained from TMM simulation, experiment, and approximation using Eq. (13).

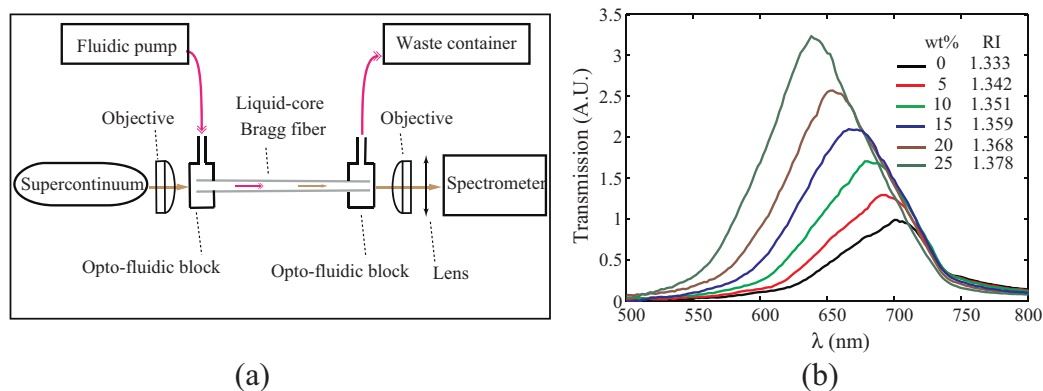


Fig. 5. (a) Schematic of the Bragg fiber sensor; (b) experimental transmission spectra of the Bragg fiber filled with NaCl solutions with different concentrations. The weight concentrations and refractive indices of the NaCl solutions are listed in the inset of (b).

ity is found to be ~ 2100 nm/RIU. Besides, Eq. (14) also indicates that the closer the value of refractive index of the fiber core to those of individual layers in the multilayer; the more sensitive the sensor will be. We, therefore, conclude that low-refractive-index-contrast Bragg fibers are generally more sensitive than their high-refractive-index-contrast counterparts [36] in sensing of liquid refractive index. Finally, one finds from (14) that sensitivity of the Bragg fiber sensor is virtually independent on the length of the fiber. In fact, centimeters-long Bragg fiber is sufficient to provide optical filtering. Therefore, short Bragg fiber pieces can be used to produce compact sensing systems which are more convenient to use, and easier to maintain than their conventional counterparts that utilize long coiled fibers.

In addition, we demonstrate the experimental implementation of this Bragg fiber sensor with the setup schematic shown in Fig. 5(a). We use two opto-fluidic blocks to integrate a 40-cm long Bragg fiber into a fluidic system. The opto-fluidic blocks are designed to simultaneously enable the optical and fluidic coupling into the core of the Bragg fiber. Each of the Bragg fiber tips is completely submerged in liquid analytes inside the block to avoid formation of air bubbles in the fiber, which would strongly suppress the fiber transmission. The Bragg fiber used in the sensor has a core diameter of ~ 0.8 mm. Such a large core results in a short response time of the sensor, since the flow resistance decreases polynomially as the core radius increases. Thus, the experimental response time of the sensor is ~ 1 s which represents an advantage of this sensor compared to other MOF sensors [37] (typical response time ~ 1 min/1 cm). The volume of liquid analytes required to fill the Bragg fiber is ~ 200 mL. To experimentally characterize the Bragg fiber sensor, we still choose the NaCl solutions with different concentrations as liquid analytes. After pumping an analyte into the Bragg fiber, we couple the beam from a supercontinuum source into the fiber. The transmission spectrum of the Bragg fiber is then analyzed by an Oriel spectrometer (Fig. 5(a)). The experimental result (Fig. 5(b)) suggests that the resonant wavelength (transmission peak) of the Bragg fiber has a blue-shift with the increasing refractive index of the fiber core, which agrees with the simulation result. Note that the propagation loss of the light within the reflector bandgap changes considerably in response to the variations in real part of analyte refractive index. For the water-filled Bragg fiber, the experimental propagation loss of the light within the reflector bandgap is typically 10–15 dB/m (at the 700 nm peak position), and the maximum sensing length of the Bragg fiber sensor is ~ 1 m.

With the linear fitting in Fig. 4, we calculate the experimental sensitivity of the sensor to be ~ 1400 nm/RIU. We note that the experimental sensitivity of the sensor is smaller than that calculated from the simulation. This is likely because in our simulation

we only take into account the HE_{11} mode, whose effective refractive index is closest in value to the refractive indices of the Bragg reflector materials, which, according to (14), makes the HE_{11} more sensitive to the changes in core index compared to other angular momentum 1 modes. In practice, due to the large diameter of the fiber core, many high order modes which are less sensitive to variations in fiber core index could be also excited, thus resulting in a smaller sensitivity. We also note that such an experimental sensitivity is comparable to that of the LPG (long period grating) MOF sensor with a sensitivity of 1500 nm/RIU [38], but smaller than that of the dual-core MOF sensor with a sensitivity of 38,000 nm/RIU [39]. However, the LPG MOF sensor requires a fiber post-processing for grating inscription while our Bragg fiber sensors enable direct measurements of analyte refractive indices. Besides, the dual-core MOF sensor is limited to liquid analytes with $n_{\text{analyte}} > n_{\text{silica}}$. Compared to these two sensors, our Bragg fiber sensor is also advantageous in its short response time (~ 1 s) due to the large core of the Bragg fiber.

4.2.2. Sensing of changes in thickness of the coated layer

Another implementation of this Bragg fiber sensor operating on the resonant sensing mode is to detect changes in thicknesses of thin layers deposited directly on the inner surface of the fiber core. By coating a thin layer, the localized refractive index in the vicinity of fiber inner surface would change substantially, which then modifies the resonant guidance of the Bragg fiber and leads to a spectral shift of the resonant wavelength in the fiber transmission. We take the thickness of the coated layer, d_a , as the measurand. Therefore, according to (7) we define the sensitivity of the Bragg fiber sensor to changes in thickness of the coated layer as: $S = \partial\lambda_c / \partial d_a$. We note that due to the large core of the Bragg fiber, only a small fraction of core-guided modes can be found in the vicinity of the inner surface of the fiber core, thus leading to a poor modal overlap of the analyte layer. Consequently, we expect the sensitivity in the surface sensing modality to be quite moderate.

To study surface sensing, we first coat a ~ 3.8 - μm thick layer on the inner surface of a 15-cm long Bragg fiber (from the same perform with the fiber used above). Particularly, a 60 wt.% sucrose solution is filled into the Bragg fiber core. Then the fiber is placed in an oven for 6 h in order to make the sucrose solution more viscous. Subsequently, an air pump is used to blow off most of the sucrose syrup in the fiber core while leaving a thin sucrose layer behind (Fig. 6(a)). The fiber is then dried again.

For the optical measurements we first insert the dry sucrose-coated Bragg fiber into the sensing setup and then quickly (~ 1 s) fill the fiber with distilled water. As the sucrose layer gradually dissolves in water, the bulk refractive index of the fiber core gradually increases. The transmission spectra (Fig. 6(b)) of the fiber

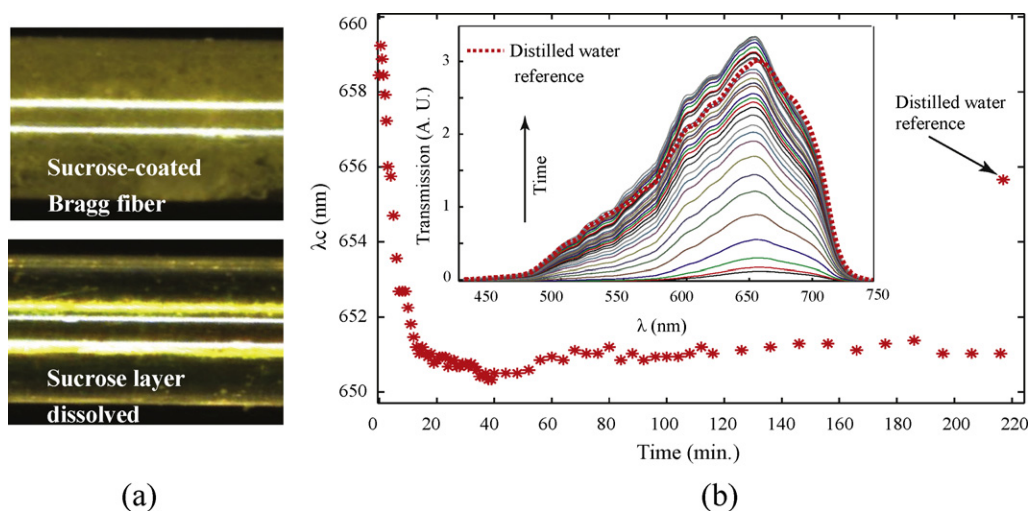


Fig. 6. (a) Top: appearance of the Bragg fiber coated sucrose layer; bottom: appearance of the Bragg fiber with the coated layer dissolved in the liquid core. (b) Time dependent spectral changes in the fiber transmission during the dissolution of a thin sucrose layer coated on the inner surface of a fiber core. At $t=0$ the fiber core is dry; sucrose layer is $3.8\ \mu\text{m}$ thick. Then, distilled water is quickly introduced. In the first 20 min rapid changes in the transmission intensity and peak position are detected. After several hours the reference is measured by purging the fiber with distilled water.

are acquired throughout the dissolution process. Fig. 6 shows that the transmission spectrum shifts $\sim 8.2\ \text{nm}$ towards shorter wavelengths in the first 20 min after filling the fiber with distilled water. During this period, the spectral shift is mostly due to increase of the bulk refractive index of the core caused by the dissolution of sucrose-layer. No significant spectral shift appears after 20 min which indicates that most of the sucrose layer is dissolved. In contrast, the transmitted intensity still keeps slowly increasing during the several hours that follow. Visual inspection of the fiber under the microscope indicates that increase of the signal amplitude is probably due to reduction of the scattering losses incurred by the fiber mode on small chunks of the undissolved sucrose. Finally, when fiber transmission spectrum stops changing (complete dissolution of the sucrose layer), we refill the fiber with distilled water. Consequently, the peak of the transmission spectrum shifted to $655.7\ \text{nm}$. Comparison with the initial peak position that is measured almost instantaneously after filling the sucrose-coated fiber with water allows us to conclude that the presence of a $3.8\text{-}\mu\text{m}$ thick sucrose layer leads to a $3.5\ \text{nm}$ red shift of the transmission spectrum of a water-filled fiber compared to that of a water-filled fiber without a sucrose layer. The corresponding surface sensitivity of our sensor to changes in the layer thickness is then estimated to be $\sim 0.9\ \text{nm}/\mu\text{m}$. Note that the sensitivity for the surface sensing, in principle, is also strongly independent on the length of the fiber; however, the maximal sensing length is experimentally found to be $\sim 20\ \text{cm}$ due to the large scattering loss caused by the sucrose layer.

5. Conclusions

We have detailed operation principles behind the analyte-filled low-refractive-index-contrast Bragg fiber-based resonant optical sensors of changes in the real part of the analyte refractive index. The sensor described in the paper showed strong resonant dependence of the fiber transmission on the real value of the analyte refractive index. A sensitivity of $\sim 1400\ \text{nm}/\text{RIU}$ is experimentally achieved, which is comparable to those of plasmonic waveguide-based sensors. Moreover, we note that maximal sensor sensitivity is largely independent of the sensor length. Finally, we demonstrate the operation of the Bragg fiber sensor in the surface sensing modality to detect changes in thicknesses of layers deposited on the inner surface of the Bragg fiber core. Only a moderate surface sensitivity

of $\sim 0.9\ \text{nm}/\mu\text{m}$ is reported due to the poor overlap of core guided modes to the deposited thin layer.

References

- [1] A. Mclean, C. Moran, W. Johnstone, B. Culshaw, D. Marsh, P. Parker, Detection of hydrocarbon fuel spills using a distributed fiber-optic sensor, *Sens. Actuators A* 109 (2003) 60.
- [2] M.E. Bosch, A.J.R. Sanchez, F.S. Rojas, C.B. Ojeda, Recent development in optical fiber biosensors, *Sensors* 70 (2007) 797.
- [3] X. Fan, I.M. White, S.I. Shapova, H. Zhu, J.D. Suter, Y. Sun, Sensitive optical biosensors for unlabeled targets: a review, *Anal. Chim. Acta* 620 (2008) 8.
- [4] N. Kim, I. Park, W. Kin, Salmonella detection with a direct binding optical grating coupler immunosensor, *Sens. Actuators B* 121 (2007) 606.
- [5] S. Balasubramanian, I.B. Sorokulova, V.J. Vodyannoy, A.L. Simonian, Lytic phage as a specific and selective probe for detection of *Staphylococcus aureus* – a surface plasmon resonance spectroscopic study, *Biosens. Bioelectron.* 22 (2007) 948.
- [6] H.J. Watts, C.R. Lowe, D.V. Pollard-Knight, Optical biosensor for monitoring microbial cells, *Anal. Chem.* 66 (1994) 2465.
- [7] D.R. Demarco, D.V. Lim, Direct detection of *Escherichia coli* o157:h7 in unpasteurized apple juice with an evanescent wave sensor, *J. Rapid Methods Autom. Microbiol.* 9 (2001) 241.
- [8] J.R. Shepard, Y. Danin-Poleg, Y. Kashi, D.R. Walt, Array-based binary analysis for bacterial typing, *Anal. Chem.* 77 (2005) 319–326.
- [9] M. Zourob, S. Mohr, B.J.T. Brown, P.R. Fielden, M.B. McDonnell, N.J. Goddard, An integrated metal clad leaky waveguide sensor for detection of bacteria, *Anal. Chem.* 77 (2005) 232–242.
- [10] L. Rindorf, J.B. Jensen, M. Dufva, L.H. Pedersen, P.E. Hoiby, O. Bang, Photonic crystal fiber long-period gratings for biochemical sensing, *Opt. Express* 14 (2006) 8224.
- [11] J.R. Ott, M. Heuck, C. Agger, P.D. Rasmussen, O. Bang, Label-free and selective nonlinear fiber-optical biosensing, *Opt. Express* 16 (2008) 20834.
- [12] M. Skorobogatiy, Resonant biochemical sensors based on photonic bandgap waveguides and fibers, in: M. Zourob, L. Akhlesh (Eds.), *Optical Guided-wave Chemical and Biosensors II*, Springer-Verlag, Berlin, Heidelberg, 2010, pp. 43–72.
- [13] J.B. Jensen, P.E. Hoiby, G. Emiljanov, O. Bang, L.H. Pedersen, A. Bjarklev, Selective detection of antibodies in microstructured polymer optical fibers, *Opt. Express* 13 (2005) 5883.
- [14] J.M. Fini, Microstructure fibres for optical sensing in gases and liquids, *Meas. Sci. Technol.* 15 (2004) 1120.
- [15] S.O. Konorov, A.M. Zheltikov, M. Scalora, Photonic-crystal fiber as a multifunctional optical sensor and sample collector, *Opt. Express* 13 (2005) 3454.
- [16] E. Pone, C. Dubois, A. Dupuis, S. Lacroix, M. Skorobogatiy, Fabrication of the hollow all-polymer Bragg fibers, in: *Proceedings of European Conference on Optical Communication*, 2006, p. We446.
- [17] B. Temelkuran, S.D. Hart, G. Benoit, J.D. Joannopoulos, Y. Fink, Wavelength-scalable hollow optical fibres with large photonic bandgaps for CO_2 laser transmission, *Nature* 420 (2002) 650.
- [18] E. Pone, C. Dubois, N. Gu, Y. Gao, A. Dupuis, F. Boismenu, S. Lacroix, M. Skorobogatiy, Drawing of the hollow all-polymer Bragg fibers, *Opt. Express* 14 (2006) 5838.

- [19] J.C. Knight, T.A. Birks, R.S.J. Russell, J.G. Rarity, Bragg scattering from an obliquely illuminated photonic crystal fiber, *Appl. Opt.* 37 (1998) 449–452.
- [20] P.S.T.J. Russell, Photonic crystal fibers, *J. Lightwave Technol.* 24 (2006) 4729–4749.
- [21] C.M. Smith, N. Venkataraman, M.T. Gallagher, D. Müller, J.A. West, N.F. Borrelli, D.C. Allan, K.W. Koch, Low-loss hollow-core silica/air photonic bandgap fibre, *Nature* 424 (2003) 657–659.
- [22] G. Vienne, Y. Xu, C. Jakobsen, H.J. Deyerl, J. Jensen, T. Sorensen, T. Hansen, Y. Huang, M. Terrel, R. Lee, N. Mortensen, J. Broeng, H. Simonsen, A. Bjarklev, A. Yariv, Ultra-large bandwidth hollow-core guiding in all-silica Bragg fibres with nano-supports, *Opt. Express* 12 (2004) 3500–3508.
- [23] A. Argyros, M.A.V. Eijkelenborg, M.C.J. Large, I.M. Bassett, Hollow-core microstructured polymer optical fiber, *Opt. Lett.* 31 (2006) 172.
- [24] J.A. Harrington, A review of IR transmitting hollow waveguides, *Fiber Integr. Opt.* 19 (2000) 211.
- [25] Y.W. Shi, K. Ito, Y. Matsuura, M. Miyagi, Multiwavelength laser light transmission of hollow optical fiber from the visible to the mid-infrared, *Opt. Lett.* 30 (2005) 2867.
- [26] Y.L. Hoo, W. Jin, H.L. Ho, L. Ju, D.N. Wang, Gas diffusion measurement using hollow-core photonic bandgap fiber, *Sens. Actuators B* 105 (2005) 183–186.
- [27] C. Charlton, B. Temelkuran, G. Delleman, B. Mizaikoff, Midinfrared sensors meet nanotechnology trace gas sensing with quantum cascade lasers inside photonic band-gap hollow waveguides, *Appl. Phys. Lett.* 86 (2005) 194102.
- [28] S.O. Konorov, A.B. Fedotov, A.M. Zheltkov, R.B. Miles, Phase-matched four-wave mixing and sensing of water molecules by coherent anti-Stokes Raman scattering in large-core-area hollow photonic-crystal fibers, *J. Opt. Soc. Am. B* 22 (2005) 2049–2053.
- [29] F.M. Cox, A. Arguros, M.C.J. Large, Liquid-filled hollow core microstructured polymer optical fiber, *Opt. Express* 14 (2006) 4135–4140.
- [30] S. Smolka, M. Barth, O. Benson, Highly efficient fluorescence sensing with hollow core photonic crystal fibers, *Opt. Express* 15 (2006) 12783–12791.
- [31] A.W. Snyder, J. Love, *Optical Waveguide Theory*, 2nd ed., Springer, 2008.
- [32] S.G. Johnson, M. Ibanescu, M. Skorobogatiy, O. Weisberg, T.D. Engeness, M. Soljacic, S.A. Jacobs, J.D. Joannopoulos, Y. Fink, Low-loss asymptotically single-mode propagation in large core omniguide fibers, *Opt. Express* 9 (2001) 748.
- [33] M. Skorobogatiy, Efficient anti-guiding of TE and TM polarizations in low index core waveguides without the need of omnidirectional reflector, *Opt. Lett.* 30 (2005) 2991.
- [34] W.M. Haynes, *CRC Handbook of Chemistry and Physics*, 91st ed., CRC Press, Boca Raton, FL, 2010, pp. 8–71.
- [35] J.M. Sullivan, M.S. Twardowski, J.R.V. Zaneveld, C.M. Moore, A.H. Barnard, P.L. Donaghay, B. Rhoades, Hyperspectral temperature and salt dependencies of absorption by water and heavy water in the 400–750 nm spectral range, *Appl. Opt.* 45 (2006) 5294.
- [36] K.J. Rowland, S. Afshar, V.A. Stolyarov, Y. Fink, T.M. Monro, Spectral properties of liquid-core Bragg fibers, in: *Conference on Lasers and Electro-Optics/International Quantum Electronics Conference*, 2009, p. CThE2.
- [37] J. Sun, C.C. Chan, Photonic bandgap fiber for refractive index measurement, *Sens. Actuators B* 128 (2007) 46.
- [38] L. Rindorf, O. Bang, Highly sensitive refractometer with a photonic-crystal-fiber long-period grating, *Opt. Lett.* 33 (2008) 563.
- [39] D.K.C. Wu, B.T. Kuhlmeiy, B.J. Eggleton, Ultrasensitive photonic crystal fiber refractive index sensor, *Opt. Lett.* 34 (2008) 322.

Biographies

Hang Qu has received his B.Sc. and M.Sc. in physics from Jilin University in 2005 and 2007, respectively. He is currently working towards a Ph.D. in engineering physics at Ecole Polytechnique de Montreal. His current fields of interest include photonic bandgap fiber sensing, capillary fiber sensing, microstructured-fiber-based devices.

Dr. Maksim Skorobogatiy has received his B.Sc. degree in physics from Rochester Institute of Technology, Rochester, USA (1995); M.Sc. in physics from McGill University, Montréal, Canada (1997); M.Sc. in electrical engineering and computer science from Massachusetts Institute of Technology (MIT), Cambridge, USA (2000); Ph.D. in physics also from MIT in 2001. During 2001–2003 he was heading a theory and simulations group at MIT startup OmniGuide Inc., where he was working on commercialization of the hollow photonic bandgap fiber technology for delivery of high power laser beams. Since 2003, he is an associate professor and a Canada Research Chair in Micro- and Nano-Photonics at Ecole Polytechnique de Montréal/University de Montréal, Canada. His current fields of interest include design and fabrication of photonic crystal fibers for sensing and telecommunications, as well as the general fields of plasmonics, and nano-photonics.